AGU PUBLICATIONS

JGR

Journal of Geophysical Research: Biogeosciences

RESEARCH ARTICLE
10.1002/2015JG003023

Key Points:
- LUE is most responsive to plant, then atmospheric and soil moisture indicators
- Top layer soil moisture best explains LUE variation for grassland ecosystems
- Single moisture function is not sufficient to capture LUE variability in all biomes

Supporting Information:
- Supporting Information S1

Correspondence to:
Y. Zhang and C. Song,
ylzhang@unc.edu;
csong@email.unc.edu

Citation:
Zhang, Y., C. Song, G. Sun, L. E. Band, A. Noormets, and Q. Zhang (2015), Understanding moisture stress on light use efficiency across terrestrial ecosystems based on global flux and remote-sensing data, *J. Geophys. Res. Biogeosci.*, *120*, 2053–2066, doi:10.1002/2015JG003023.

Received 15 APR 2015
Accepted 20 SEP 2015
Accepted article online 25 SEP 2015
Published online 21 OCT 2015

Understanding moisture stress on light use efficiency across terrestrial ecosystems based on global flux and remote-sensing data

Yulong Zhang[1,2], Conghe Song[1,3], Ge Sun[4], Lawrence E. Band[1,2], Asko Noormets[4,5], and Quanfa Zhang[6]

[1]Department of Geography, University of North Carolina, Chapel Hill, North Carolina, USA, [2]Institute for the Environment, University of North Carolina, Chapel Hill, North Carolina, USA, [3]School of Ecological and Environmental Sciences, East China Normal University, Shanghai, China, [4]Eastern Forest Environmental Threat Assessment Center, Southern Research Station, USDA Forest Service, Raleigh, North Carolina, USA, [5]Department of Forestry and Environmental Resources, North Carolina State University, Raleigh, North Carolina, USA, [6]Key Laboratory of Aquatic Botany and Watershed Ecology, Wuhan Botanical Garden, Chinese Academy of Sciences, Wuhan, China

Abstract Light use efficiency (LUE) is a key biophysical parameter characterizing the ability of plants to convert absorbed light to carbohydrate. However, the environmental regulations on LUE, especially moisture stress, are poorly understood, leading to large uncertainties in primary productivity estimated by LUE models. The objective of this study is to investigate the effects of moisture stress on LUE for a wide range of ecosystems on daily, 8 day, and monthly scales. Using the FLUXNET and Moderate Resolution Imagine Spectroradiometer data, we evaluated moisture stress along the soil-plant-atmosphere continuum, including soil water content (SWC) and soil water saturation (SWS), land surface wetness index (LSWI) and plant evaporative fraction (EF), and precipitation and daytime atmospheric vapor pressure deficit (VPD). We found that LUE was most responsive to plant moisture indicators (EF and LSWI), least responsive to soil moisture (SWC and SWS) variations with the atmospheric indicator (VPD) falling in between. LUE showed higher sensitivity to SWC than VPD only for grassland ecosystems. For evergreen forest, LUE had better association with VPD than LSWI. All moisture indicators (except soil indicators) were generally less effective in affecting LUE on the daily and 8 day scales than on the monthly scale. Our study highlights the complexity of moisture stress on LUE and suggests that a single moisture indicator or function in LUE models is not sufficient to capture the diverse responses of vegetation to moisture stress. LUE models should consider the variability identified in this study to more realistically reflect the environmental controls on ecosystem functions.

1. Introduction

As the initial carbohydrate produced by plant through photosynthesis, terrestrial gross primary productivity (GPP) is the largest CO_2 flux in the global carbon cycle and a key driver of ecosystem functions, such as respiration and growth [*Beer et al.*, 2010]. Ecosystem GPP minus autotrophic respiration not only dictates the carbon balance of land surface [*Nemani et al.*, 2003] but also maintains the food chain for all life and defines the planetary boundary for human habitation on the planet [*Running*, 2012]. Therefore, it is of major scientific significance to accurately estimate terrestrial GPP [*Song et al.*, 2013; *Anav et al.*, 2015]. Since carbon and water cycles are tightly coupled, accurately estimating GPP also has importance in quantifying water balances and carbon-water tradeoffs in ecosystem service assessment [*Sun et al.*, 2011].

Although numerous models estimating GPP have been developed in the past decades, large discrepancies in GPP estimation still exist due to the deficiency in characterizing the environmental regulations [*Schaefer et al.*, 2012; *Piao et al.*, 2013; *Yuan et al.*, 2014]. Light use efficiency (LUE) is a key biophysical parameter indicating the ability of plants to convert absorbed light energy to chemical energy through photosynthesis [*Medlyn*, 1998]. Among those prognostic models, GPP models based on LUE using remotely sensed data from space-borne satellites are considered to have high potential to map the spatial-temporal dynamics of GPP because of its simplicity and the solid biophysical linkage between the fraction of absorbed photosynthetically active radiation and remotely sensed spectral signals [*Monteith*, 1972; *Asrar et al.*, 1984; *Potter et al.*, 1993; *Yuan et al.*, 2007; *Song et al.*, 2013]. However, the environmental regulations on LUE, especially from moisture, have relatively large uncertainties [*Xiao et al.*, 2004; *Schaefer et al.*, 2012; *Yuan et al.*, 2014], which constrain the accuracy of GPP estimated with LUE-based models.

Table 1. Flux Tower Data Usage for Different Biomes on Daily, 8 Day, and Monthly Scales

		Daily		8 Day		Monthly	
IGBP Biomes[a]	MODIS FPAR/LAIBiomes[b]	No. of Flux Towers	Total Data Records[d]	No. of Flux Towers	Total Data Records[d]	No. of Flux Towers	Total Data Records[d]
ENF	ENF	51	10065	27	914	5	133
EBF	EBF	12	3597	10	347	4	58
DBF	DBF	20	5133	14	491	4	82
MF	Forest[c]	9	1222	4	94	1	11
SHR	SHR	5	1441	4	225	3	61
SAV	SAV	7	2644	5	360	5	113
GRA	GCC	24	1983	7	174	1	20
CRO	GCC/BC	26	3257	10	374	6	76
Total		154	29342	81	2979	29	554

[a]IGBP Biome abbreviations: ENF (evergreen needleleaf forest), EBF (evergreen broadleaf forest), DBF (deciduous broadleaf forest), MF (mixed forest), SHR (close shrub and open shrub), SAV (savannas and woody savannas), GRA (grassland), and CRO (cropland).
[b]MODIS FPAR/LAI Biome abbreviations: GCC (grass/cereal crop), BC (broadleaf crop); others are same as IGBP.
[c]Since MODIS FPAR/LAI Biomes do not include MF, "Forest" here indicate all the other forest types except MF in IGBP.
[d]The data records here are shown for the availability of calculated LUE. The records for other moisture indicators may be different.

Due to global warming and the associated enhanced variability of precipitation, drought events have become more frequent [*Vicente-Serrano et al*., 2013], significantly influencing terrestrial primary productivity [*Ciais et al*., 2005; *Zhao and Running*, 2010; *Zhang et al*., 2014]. To quantify water stress, different moisture scalars have been incorporated in LUE models. For example, the Moderate Resolution Imagine Spectroradiometer (MODIS) GPP algorithm used daytime vapor pressure deficit (VPD) to account for moisture stress on LUE [*Zhao and Running*, 2010]; the 3PG [*Landsberg and Waring*, 1997] and CFLUX [*King et al*., 2011] models both adopted VPD and soil water content (SWC) to quantify moisture stress; the VPM model used satellite-based land surface water index (LSWI) to account for moisture stress [*Xiao et al*., 2004]; and the eddy covariance (EC)-LUE model used the evaporative fraction (EF) to characterize moisture stress [*Yuan et al*., 2007]. However, LUE models generally calibrate the environmental scalars (including moisture stress) on LUE by minimizing the overall root-mean-square error to match the GPP derived from eddy covariance flux tower measurements. This treatment could produce relatively accurate GPP at the flux tower sites, but may not retain the actual relationship between the specific factor (e.g., moisture) and LUE, which is a typical modeling problem: getting the right answer for the wrong reason.

The soil-plant-atmosphere continuum (SPAC) describes the pathway of water movement from soil through plant to the atmosphere [*Tuzet et al*., 2003]. The change of water content in each interface could alter the water potential gradient along SPAC, which further influences the carbon gain efficiency of vegetation [*Williams et al*., 2001]. In this study, we investigated the moisture stress from three groups of indicators along SPAC (i.e., atmosphere, soil, and plant) on LUE across terrestrial ecosystems. To achieve this objective, we used global eddy covariance (EC) flux data and remotely sensed data from MODIS. We first applied a series of data screenings to minimize the influences from unrelated environmental factors on realized LUE, and further ensured the land cover consistency between the local tower footprint and the overlying satellite data. We conducted the analysis of LUE with different moisture indicators on three temporal scales, daily, 8 day, and monthly, for a total of eight vegetation types.

2. Materials and Methods

2.1. Global Site Level Database

We combined worldwide EC flux data and site level remote-sensing data, and built up a global database for eight biomes on three temporal scales (i.e., daily, 8 day, and monthly) (Table 1). In this data set, the flux-tower-based or in situ observations include GPP ($g\,C\,m^{-2}\,d^{-1}$), incident short-wave radiation ($MJ\,m^{-2}\,d^{-1}$), precipitation ($mm\,d^{-1}$), daily maximum air temperature (°C), daily minimum air temperature (°C), daytime vapor pressure deficit (VPD) (hPa), soil water content in the upper layer (~0.3 m), latent heat ($MJ\,m^{-2}\,d^{-1}$), and sensible heat ($MJ\,m^{-2}\,d^{-1}$); biophysical parameters derived from remotely sensed data

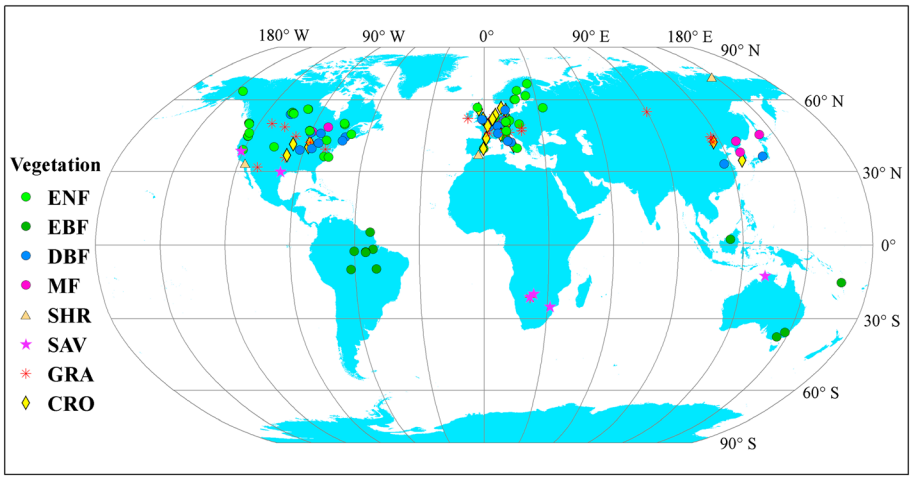

Figure 1. Geographical and biome information of FLUXNET tower sites used in this study. Biome abbreviations are given in Table 1.

from MODIS include fraction of absorbed photosynthetically active radiation (FPAR), leaf area index (LAI), and land surface wetness index (LSWI); other site information include location, biome type, soil water field capacity, and wilting point.

The EC flux data were from FLUXNET Synthesis Data Set, which harmonized and gap filled the half-hourly records of carbon dioxide, water vapor, and energy fluxes over 253 eddy covariance towers from 2000 to 2007 (http://www.fluxdata.org/). These sites spanned a wide range of climate and physiographic regions from 70°N to 37°S and included major terrestrial ecosystems defined by the International Geosphere Biosphere Programme (IGBP) classification: evergreen needleleaf forest (ENF), evergreen broadleaf forest (EBF), deciduous broadleaf forest (DBF), mixed forest (MF), shrubland (SHR), savannas (SAV), grassland (GRA), and cropland (CRO) (Figure 1). FLUXNET sites used in this study did not have deciduous needleleaf forest and crop/natural vegetation mosaic. Due to site limitation, we combined close shrub and open shrub as SHR and savannas and woody savannas as SAV in this study. In the FLUXNET data set, the daily data were integrated from the gap-filled half-hourly data [*Agarwal et al*., 2010]. We further scaled the daily data to 8 day and monthly averages. Data with the missing proportion higher than 20% on the 8 day and monthly scales were excluded in the analysis. The FPAR, LAI, and LSWI data for each tower site from 2000 to 2007 were derived from 8 day 1×1 km MODIS product (MOD15A2 C5) and 500×500 m MODIS reflectance data (MOD09A1 C5), respectively. These data were downloaded from the Oak Ridge National Laboratory Archive Center (http://daac.ornl.gov/MODIS/MODIS-menu/modis_webservice.html). Only data from the pixel containing the flux tower were used. The smoothing and interpolation of these MODIS-based variables from 8 day to daily and monthly scales are present in the following sections.

2.2. LUE Calculation

Light use efficiency (LUE) refers to the amount of carbon fixed per unit of absorbed photosynthetically active radiation (APAR) by vegetation, which is defined as the ratio of GPP to APAR as

$$\mathrm{LUE} = \frac{\mathrm{GPP}}{\mathrm{APAR}} = \frac{\mathrm{GPP}}{\mathrm{PAR} \times \mathrm{FPAR}} \tag{1}$$

where PAR is the incident photosynthetically active radiation (MJ m^{-2} d^{-1}), which is assumed to be 45% of the downward short-wave radiation in this study [*Campbell and Norman*, 2012]; FPAR is the fraction of PAR being absorbed by the plants.

GPP and incident radiation were obtained from the global flux data. It is important to note that flux-tower-based GPP was not strictly in situ observation, but indirectly derived from the measured net ecosystem exchange and estimated ecosystem respiration, which carry uncertainties [*Reichstein et al*., 2005]. FPAR was from the above mentioned MODIS product (MOD15A2), which is an 8 day composite based on the maximum values of daily FPAR and LAI. The main biophysical retrieval algorithm for MOD15A2 is to use

a biome-specific lookup table derived from a three-dimensional radiative transfer model (RTM) to calculate the most probable values of FPAR as well as LAI for each pixel [*Knyazikhin et al*., 1999; *Myneni et al*., 2002]. The RTM inputs include an eight-biome classification map, daily atmospherically corrected surface reflectance from red and near-infrared bands, and associated scene Sun sensor geometry, while the RTM outputs are the instantaneous FPAR and LAI at the time of satellite overpass (i.e., local time 10:30 A.M.) [*Myneni et al*., 2002; *Serbin et al*., 2013]. If the main algorithm fails due to bad geometry, cloud contamination or snow/ice, a backup algorithm based on the relationship between normalized difference vegetation index (NDVI) and FPAR/LAI is adopted. However, the FPAR/LAI retrieved by backup algorithm is usually not reliable due to the poor quality of input data (i.e., NDVI) in such situations [*Zhao et al*., 2005]. In this study, we examined the Quality Flag (QC), and excluded the data with bad quality for each site (i.e., backup algorithm or filled values). Based on the good quality data (i.e., RTM algorithm), we filled the temporal gaps and smoothed the 8 day FPAR/LAI data using the double logistic method in the software package of TIMSAT 3.1 [*Jönsson and Eklundh*, 2004]. The 8 day smoothed FPAR and LAI data were further interpolated to the monthly data using the time-weighted average. Since we could not extract the meaningful daily information from the maximum composite data during the 8 day period, we assumed the daily FPAR constant within the 8 day period. It should be noted that FPAR depends on the solar zenith angle (SZA) and shows a diurnal variation pattern. Using the instantaneous MODIS FPAR as representative of the daily or even longer-term FPAR may add uncertainty into the LUE calculation, although this is a common way in current LUE models, e.g., MODIS GPP [*Zhao and Running*, 2010] and CFLUX [*King et al*., 2011]. Usually, it may lead to the overestimation of LUE due to the underestimation of FPAR at lower SZA. However, the overestimation of LUE may be reduced because the tower-based GPP is generally underestimated [*Reichstein et al*., 2005]. Numerical simulation suggests that SZA-related variations in MODIS FPAR are considerably weaker in dense heterogeneous canopies due to the counteraction of spatial heterogeneity over the pixel [*Shabanov et al*., 2003]. In situ measurements from a semiarid grassland showed that daily averages of FPAR calculated from 9:00 A.M. to 3:00 P.M. approximated well the values at 10:30 A.M. (corresponding to MODIS overpass time) [*Fensholt et al*., 2004]. Based on the above limited evaluations, we considered it reasonable to use MODIS FPAR to calculate LUE in this study.

2.3. Moisture Stress Indicators

2.3.1. Atmospheric Moisture Indicators

Atmospheric moisture indicators included precipitation and daytime averaged vapor pressure deficit (VPD). The daytime period was determined by hour angles of local sunset and sunrise. To consider the lag effects of precipitation on daily LUE, we further calculated the past 8 day, 30 day, and 60 day running means of precipitation.

2.3.2. Soil Moisture Indicators

Soil moisture indicators included the volumetric soil water content (SWC, $m^3\,m^{-3}$) measured at the flux tower site in the upper layer (~0.30 m) and the soil water saturation (SWS, %) defined as follows:

$$\mathrm{SWS} = \frac{\mathrm{SWC} - \mathrm{WP}}{\mathrm{FC} - \mathrm{WP}} \tag{2}$$

where FC and WP are the volumetric ($m^3\,m^{-3}$) soil water field capacity (at soil water potential of −33 kPa) and permanent wilting point (at soil water potential of −1500 kPa), respectively. Since not all flux tower sites had soil texture data, we derived WP and FC for each site from an up-to-date global high-resolution soil data set (1 × 1 km) which harmonized various published soil databases [*Wei et al*., 2014]. We averaged the values in the upper soil layers (i.e., 0–0.29 m, four of eight layers) to obtain WP and FC. In the FLUXNET data set, SWC for several sites were questionable with values exceeding 90% probably due to measurement errors or mismatching SWC units (e.g., degree of water saturation versus volumetric water content). We dropped the daily SWC values for the whole year on a specific site if any SWC value during that period was over 70%. For SWS, we excluded the values greater than 1 or less than 0.

To investigate the nonlinearity of LUE in response to SWC, we calculated the base 10 logarithm of SWC ($\log_{10}(\mathrm{SWC})$) and the nonlinear soil moisture scalar function used in the 3PG model [*Landsberg and Waring*, 1997], which is defined as follows:

$$\mathrm{SWC}_{3\mathrm{PG}} = \frac{1}{1 + \left[(1 - \mathrm{SWC}/\mathrm{FC})/C1\right]^{C2}} \tag{3}$$

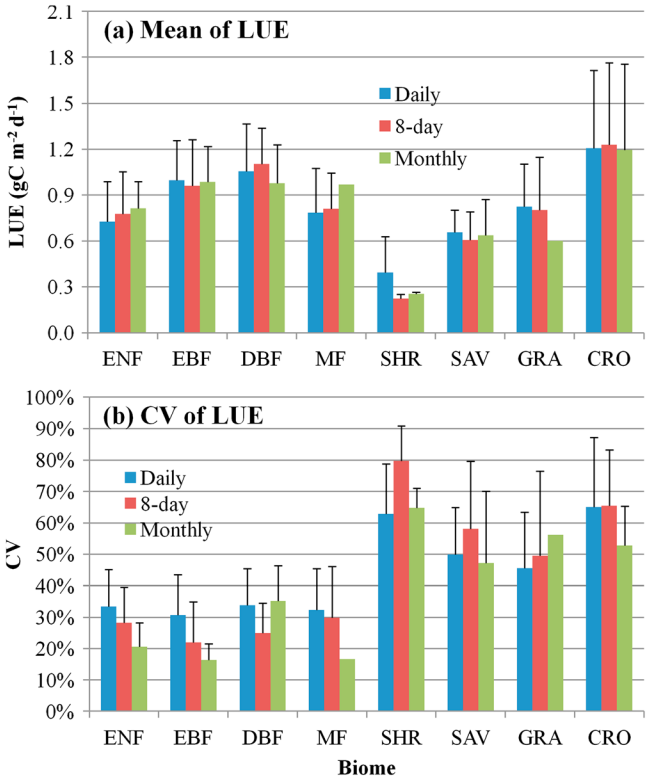

Figure 2. (a) Means and (b) variations of realized LUE stressed by moisture for different biomes on daily, 8 day, and monthly scales. Biome abbreviations are given in Table 1. CV in Figure 1b is the coefficient of variation defined as the ratio of standard deviation to the mean. The black error bar indicates the magnitude of 1 standard deviation. The statistics in Figures 1a and 1b were both derived from the averaged values for all flux tower sites within a given biome. The error bar for the biome with only one site is not shown.

where C1 and C2 are soil texture-specific parameters. In the 3PG model, the soil texture was classified into four types, i.e., clay, clay loam, sandy loam, and sandy. The proportions of sand, silt, and clay for each site were extracted from the above mentioned global 1×1 km soil data set [*Wei et al.*, 2014]. These soil components were used to determine the corresponding soil texture by the USDA textural triangle (http://www.nrcs.usda.gov/wps/portal/nrcs/detail/soils/survey/?cid=nrcs142p2_054167).

2.3.3. Plant Moisture Indicators

Plant moisture indicators included MODIS-based land surface water index (LSWI) and flux-tower-based evaporative fraction ratio (EF). The LSWI was calculated as follows:

$$\mathrm{LSWI} = \frac{\rho_{\mathrm{nir}} - \rho_{\mathrm{swir}}}{\rho_{\mathrm{nir}} + \rho_{\mathrm{swir}}} \tag{4}$$

where ρ_{nir} and ρ_{swir} are surface reflectance in near-infrared and shortwave infrared bands from the 8 day MOD09A1, respectively. Unlike FPAR and LAI, cloud-contaminated LSWI cannot be smoothed because it is influenced by synoptic weather conditions. We masked out all the records with clouds, cloud shadows and aerosols to get the 8 day high-quality LSWI. We then extracted the specific acquisition date for each 8 day record to obtain the daily LSWI. We averaged all the 8 day high-quality records within a month (at least two records required) to calculate the monthly LSWI.

EF indicates the proportion of available energy used as latent heat (or evapotranspiration), which is defined as [*Crago*, 1996]:

$$\mathrm{EF} = \frac{L}{L + H} \tag{5}$$

where L and H are latent and sensible heats, respectively. For EF, we excluded the values greater than 1 or less than 0 from the data set.

2.4. Analysis Methods

To minimize the confounding effects from unrelated environmental factors in analyzing the relationships between LUE and moisture stress indicators, we applied a series of steps on three temporal scales to screen the data potentially influenced by rainfall, diffuse radiation, high and low temperatures. Since eddy flux instruments do not function well during rainfall events, and flux data was mainly gap filled during this period [*Reichstein et al.*, 2005], we dropped the records with daily precipitation higher than 5 mm d^{-1}. The increase of diffuse radiation on overcast sky conditions could increase LUE and counteract the effect of moisture stress [*King et al.*, 2011]. To keep a relatively steady sky condition, we only included the records on each temporal scale with clear-sky index (i.e., ratio of actual to potential radiation) higher than 70%. Temperatures that are too high or low could significantly influence the realized LUE [*Ruimy et al.*, 1999]. We excluded the records with averaged daily maximum temperature higher than 35°C or with averaged daily minimum

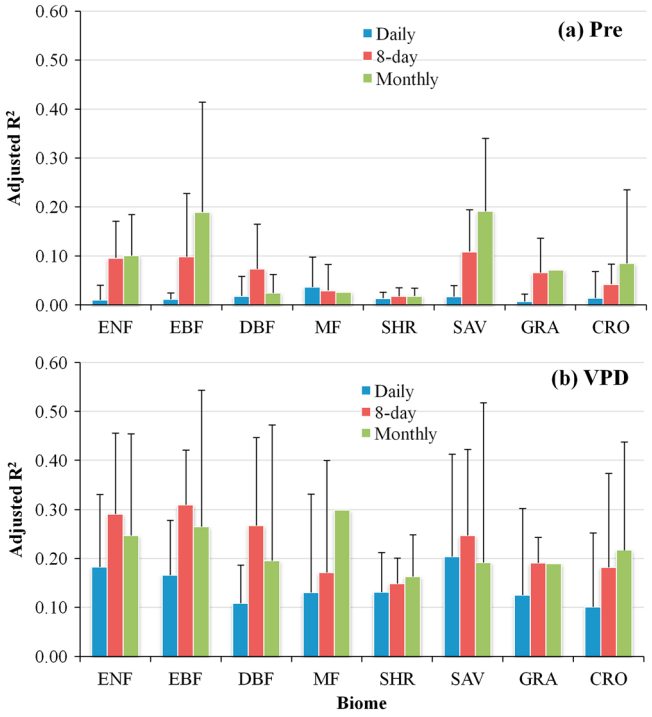

Figure 3. Adjusted R^2 between LUE and atmospheric moisture indicators of (a) precipitation (Pre) and (b) daytime vapor pressure deficit (VPD) for different biomes on daily, 8 day, and monthly scales. Biome abbreviations are given in Table 1. The black error bar indicates the magnitude of 1 standard deviation. The error bar for the biome with only one site is not shown.

temperature lower than the biome-dependent threshold of minimum temperature [*Zhao and Running*, 2010]. After the data screening, we dropped the flux tower sites with records not enough to conduct reliable statistical analysis (i.e., $n < 10$).

MODIS FPAR/LAI data used in this study were produced based on an independent MODIS land cover data [*Myneni et al.*, 2002]. Due to classification and geolocation errors, there might be potential land cover inconsistency between the local tower footprint and the overlying MODIS data. In this study, we further examined this problem by matching these two kinds of classifications (Table 1). The vegetation type over each FLUXNET site was provided by its local investigator, which is defined from the 12 biome IGBP classification, while the land cover used to derive MODIS FPAR/LAI is a coarse eight-biome classification [*Friedl et al.*, 2010]. Compared with IGBP, the FPAR/LAI classification includes the unique types of broadleaf crop (BC) and grass/cereal crop (GCC), but does not include MF. Here we regarded CRO in IGBP as BC and GCC, GRA as GCC, and MF as other forest types in FPAR/LAI (Table 1). Those sites that did not pass the biome consistency test (about 28.4% of total sites) were dropped. MODIS FPAR/LAI classification information for each site was obtained from the public website of FLUXNET at Oak Ridge National Lab (http://fluxnet.ornl.gov/).

The final usage of flux data on three temporal scales was summarized in Table 1 (final chosen EC sites were given in Table S1 in the supporting information). In general, there are more data records on the daily scale (61% of total sites) than those on the 8 day (32% of total sites) and monthly (11% of total sites) scales, while ENF, DBF, and CRO have more records than other biomes. Based on this database, we used Pearson's correlation (R) to determine the strength of association between LUE and moisture stress indicators. The coefficient of determination (R^2) provides a measure of how well the independent variable explained the variations of dependent variable. However, it is influenced by the sample size. After a series of data screenings, the data records for different moisture indicators on each flux site may be different. In this paper, we calculated sample size-scaled R^2 (i.e., adjusted R^2 or R^2_{adj}) between LUE and different indicators, and then analyzed the mean and standard deviation of R^2_{adj} within and among different biomes on three temporal scales. The R^2_{adj} is defined as follows:

$$R^2_{adj} = 1 - \left(1 - R^2\right) \times \frac{n-1}{n-p-1} \tag{6}$$

where n is the sample size, p is the number of independent variables (here p is 1).

3. Results

3.1. LUE Variations

Site-based statistics showed that CRO had the highest LUE among all the biomes analyzed, followed by forests and GRA, while SHR and SAV tended to have the lowest LUE (Figure 2a). The fact that CRO had the

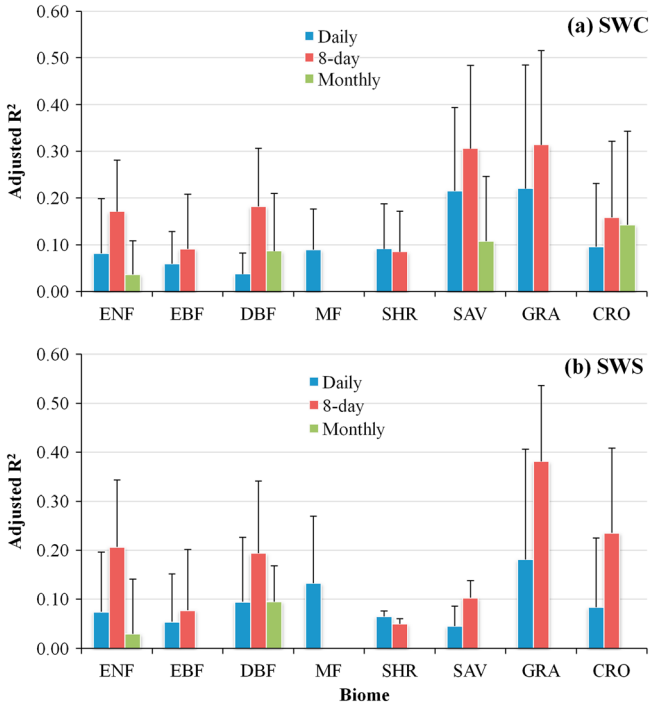

Figure 4. Adjusted R^2 between LUE and soil moisture indicators of (a) soil water content (SWC) and (b) soil water saturation (SWS) for different biomes on daily, 8 day, and monthly scales. Biome abbreviations are given in Table 1. The black error bar indicates the magnitude of 1 standard deviation. The error bar for the biome with only one site is not shown. Please note that due to more strict screenings, some SWC/SWS time series on the 8 day and monthly scales were not kept. Therefore, the bars for the relevant biomes are missing. For SWS, we excluded the values greater than 1 or less than 0, thus SWS usually had fewer records than SWC.

highest LUE may be due to the presence of C4 vegetation and management (e.g., irrigation and/or fertilization). Of the forest types, DBF showed the highest LUE. Due to the substantial within-biome variations, most noncrop vegetation had more or less similar LUE. However, the variations of LUE stressed by moisture in terms of coefficient of variation (CV, the ratio of standard deviation to the mean) were lower in forests than nonforest vegetation (Figure 2b). CRO as well as most forests generally showed lower variations of LUE on the monthly scale than that on the daily and 8 day scales (Figure 2b).

3.2. Atmospheric Indicators

Precipitation explained the variations of LUE for all biomes poorly, with averaged R^2_{adj} less than 10% on daily and 8 day scales, and less than 20% on monthly scale (Figure 3a). This probably is because not much precipitation variation was allowed in the data. We further discussed the lag effect of precipitation on LUE later in section 4. Compared with precipitation, VPD had stronger association with LUE for most biomes, but had larger variations in R^2_{adj} within biomes (Figure 3b). VPD explained variations of LUE in evergreen forest (ENF and EBF) better than DBF, while SAV better than GRA, CRO, and SHR. Overall, VPD explained the variations of LUE for most biomes better on the monthly and 8 day scales than on the daily scale, which was similar with precipitation.

3.3. Soil Indicators

On the daily and 8 day scales, SWC explained LUE variations better in GRA and SAV than that in other biomes in terms of R^2_{adj} (Figure 4a). After normalization by soil texture parameters, SWS generally showed the similar R^2_{adj} in explaining LUE variations with SWC (Figure 4b). After data screening, both SWC and SWS had sparse data on the monthly scale. Based on the limited observations, the available biomes showed no substantial differences in R^2_{adj} between LUE and SWC/SWS on monthly scale. Although there were relatively large variations in the strength of the LUE ~ SWC relationships within biomes, SWC as well as SWS generally explained LUE variations better on the 8 day scale than that on the daily and monthly scales.

3.4. Plant Indicators

LSWI generally showed stronger relationships with LUE in CRO and SAV than other nonforest biomes (Figure 5a). For forests, LSWI better explained LUE variations in DBF than that in other types probably due to a larger amount of variation in canopy moisture content for DBF. R^2_{adj} between LUE and LSWI were generally higher on 8 day and monthly scales than on daily scale for most biomes (Figure 5a). It is interesting to note that remote-sensing-based LSWI and flux-tower-based EF generally showed similar variations of R^2_{adj} among biomes, although the latter explained the variations of LUE better than the former (Figure 5b). MF tended to have the lowest R^2_{adj} for the LUE ~ EF relationship among the biomes, which might be caused by its canopy heterogeneity.

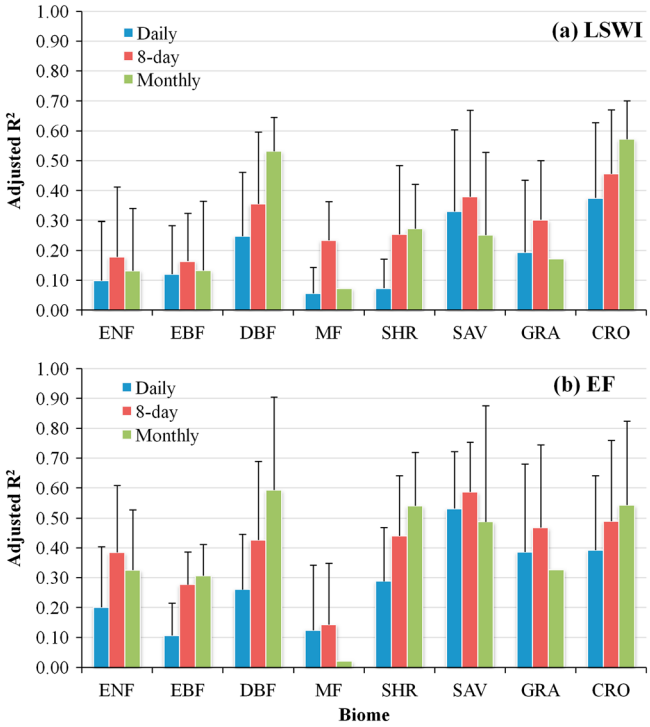

Figure 5. Adjusted R^2 between LUE and plant moisture indicators of (a) land surface water index (LSWI) and (b) evaporative fraction (EF) for different biomes on daily, 8 day, and monthly scales. Biome abbreviations are given in Table 1. The black error bar indicates the magnitude of 1 standard deviation. The error bar for the biome with only one site is not shown.

3.5. Comparison Among Indicators

For all biomes, the strengths of association between moisture indicators on LUE as measured by R^2_{adj} were ranked as EF > LSWI > VPD > SWC > SWS > Precipitation (Figure 6). The atmospheric and plant moisture indicators explained the variations of LUE better on the monthly scale, while soil moisture indicators explain the variation of LUE better on the 8 day scale (Figure 6). We selected three representative indicators (i.e., VPD for atmosphere, SWC for soil, and LSWI for plant) and compared their relationships with daily LUE among three biomes (i.e., ENF (deep rooted), GRA (shallow rooted), and CRO (managed)) along the gradients of multiyear averaged precipitation and LAI (Figure 7). Each data point in Figure 7 is an R^2_{adj} value between LUE and a moisture indicator on the daily scale for a given flux tower site. The lines in Figure 7 indicate the trend of relationships between daily LUE and moisture indicators along either the precipitation or LAI gradient. For ENF (Figures 7a and 7d), the VPD line (red) is above the SWC (blue) and LSWI (green) lines along the precipitation and LAI gradients, indicating daily LUE of ENF, is more responsive to VPD compared to SWC and LWSI. Interestingly, the relationship of daily LUE and VPD does not seem to change with precipitation. The trend line for the relationship between VPD and daily LUE for GRA is below those of SWC and LSWI (Figures 7b and 7e), indicating that VPD has the weakest effects on LUE. For GRA, daily LUE is most responsive to SWC, and the relationship is stronger at wetter sites. SWC stress on CRO is low (Figure 7c), probably due to the practice of irrigation, while LSWI is most strongly related to daily LUE of CRO along the precipitation and LAI gradients. Through the comparative analysis in Figure 7, we found that the same moisture stressor has different effects on daily LUE for different biomes. Among VPD, SWC, and LSWI, VPD has the strongest control on daily LUE for ENF, SWC on GRA, and LSWI on CRO along either the precipitation or LAI gradient.

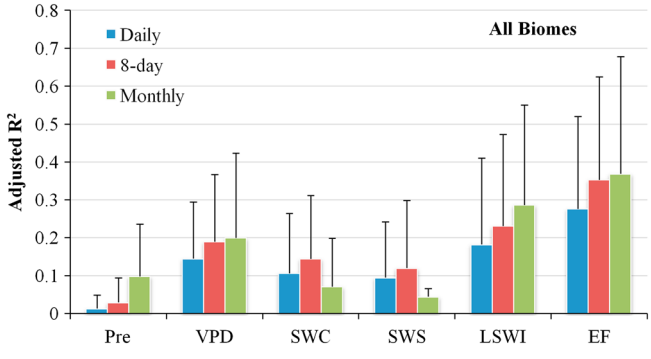

Figure 6. Adjusted R^2 between LUE and three groups of moisture indicators for all biomes on daily, 8 day, and monthly scales. Atmosphere indicators: precipitation (Pre), and daytime vapor pressure deficit (VPD); Soil indicators: volumetric soil water content (SWC) and soil water saturation (SWS); Plant indicators: land surface water index (LSWI) and evaporative fraction (EF). The black error bar indicates the magnitude of 1 standard deviation.

4. Discussion

Terrestrial ecosystems adopt divergent strategies to minimize drought costs (e.g., defoliation to avoid dehydration versus stomatal closure to tolerate drought) [*Bacelar et al.*, 2012]. By correlating remotely sensed vegetation index and drought indicators,

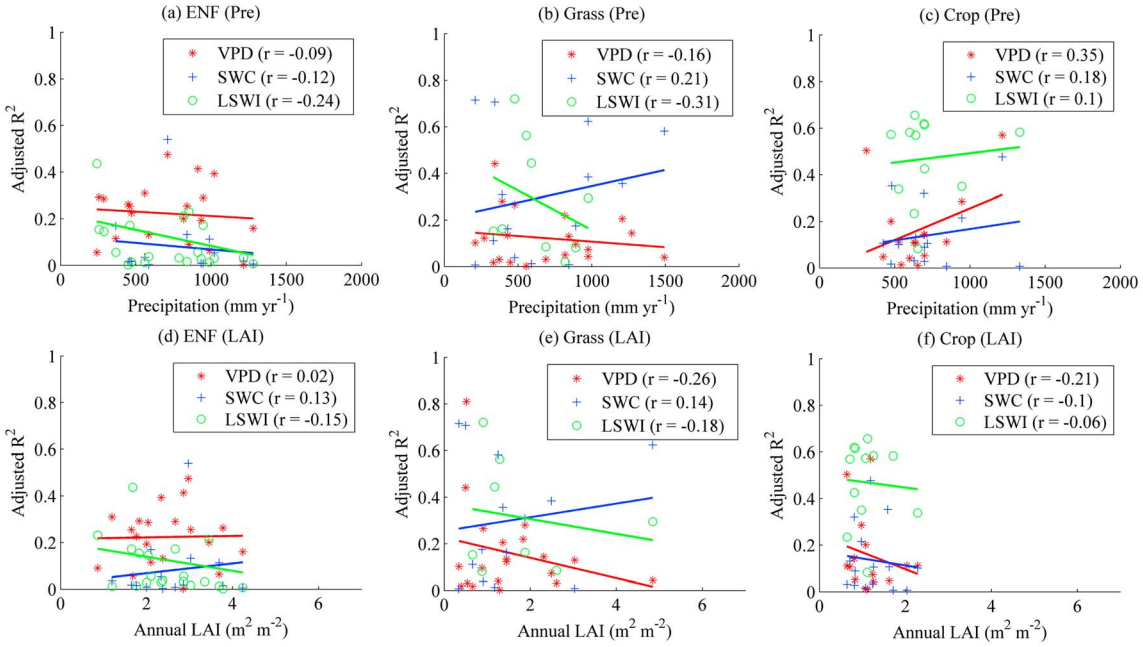

Figure 7. Comparisons of site-based adjusted R^2 between daily LUE and representative moisture stress indicators for three biomes (evergreen needleleaf forest (ENF), Grass, Crop) (a–c) along the gradients of multiyear averaged precipitation (Pre) and (d–f) leaf area index (LAI). Atmosphere indicators: daytime vapor pressure deficit (VPD); Soil indicators: soil water content (SWC); Plant indicators: land surface water index (LSWI). Red, blue, and green lines are the linear fits for VPD, SWC, and LSWI, respectively. The value in parenthesis in the legend is the Pearson's Correlation between adjusted R^2 and precipitation and LAI for all sites. Multiyear averaged precipitation and LAI are derived from flux tower data and smoothed MODIS LAI, respectively.

Sims et al. [2014] found that forested ecosystems had less changes in canopy greenness with drought than nonforested ecosystems, probably due to the stored water in the stems and water accessibility via deep roots. Site-based studies using data from eddy covariance flux towers in forest ecosystems also indicated that extreme and lasting soil water stress are rare to significantly reduce seasonal ET and GPP [*Xie et al*., 2014; *Fang et al*., 2015]. Our study further confirmed that besides canopy greenness, forest LUE was also less sensitive to water stress than nonforest biomes (Figure 2b).

Vegetation conducts photosynthesis at the cost of losing water to the atmosphere [*Churkina et al*., 1999]. Moisture stress or physiological drought for plant would happen when there is an imbalance between water demand and water storage in the plant [*McDowell et al*., 2008]. In this study, we comprehensively examined the relationships between LUE and these three groups of moisture indicators. We found that these indicators showed great variations in quantifying moisture stress on LUE across different terrestrial ecosystems (Figures 3–7). Of atmosphere indicators, precipitation, as the major source of water for SPAC, could influence all the other moisture indicators during short- or long-term period and impose indirect influences on LUE [*Siqueira et al*., 2009]. However, our study showed that low precipitation (i.e., < 5 mm d^{-1}) had weak links with LUE variations on daily, 8 day, and monthly scales for all biomes (Figure 3a). Due to the data screening in our study, we could not examine the effects of moderate and high precipitation (i.e., > 5 mm d^{-1}) on LUE. Here we further examined the lag effects (i.e., past 8 day, 30 day, and 60 day) of precipitation on daily LUE as an alternative (Figure 8). Our results showed substantial lag effects of past precipitation on LUE for most biomes, especially for SAV and GRA (Figure 8), suggesting the indirect mechanism of precipitation in affecting plant growth during the long-term period [*Wu and Chen*, 2012].

VPD, as an evaporative demand of SPAC, could affect plant growth by controlling the openness of leaf stomata [*Ocheltree et al*., 2014]. Our study clearly showed that LUE was more sensitive to changes in VPD than in precipitation on daily, 8 day, and monthly scales (Figure 3). However, VPD may decouple with soil water dynamics due to its oversensitivity to temperature, especially in summer monsoon regions [*Mu et al*., 2007], suggesting that the lag effect of precipitation may potentially influence the relationship between VPD and LUE. Plant indicators including LSWI and EF were shown to have the closest association with LUE for most ecosystems (Figures 5 and 6), suggesting that they should be the priority of moisture scalar

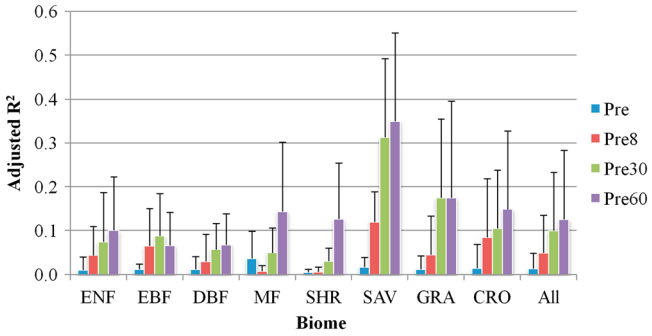

Figure 8. Adjusted R^2 between daily LUE and precipitation with different lag times for different biomes. Pre: daily precipitation; Pre8, Pre30, and Pre60 are past 8 day, 30 day, and 60 day running means of daily precipitation. Biome abbreviations are given in Table 1. The black error bar indicates the magnitude of 1 standard deviation.

selection in LUE models [*Garbulsky et al*., 2010]. However, the unavailability of EF over space and the frequent cloud contamination in LSWI constrain the applications of plant indicators in LUE models [*Xiao et al*., 2004; *Yuan et al*., 2007]. In such case, VPD could be used as a good surrogate to fill the spatiotemporal gaps of plant indicators. Our study further found that LSWI showed worse performance in explaining daily LUE variations than VPD in evergreen forests (Figures 3, 5, and 7), probably because evergreen forests have relatively small seasonal variations in canopy water content measured by remote-sensing signals compared with other biomes. It suggests that the GPP estimation of evergreen forests may improve when integrating VPD into those LUE models that used LSWI as the only moisture scalar (e.g., VPM [*Xiao et al*., 2004]).

Observed LUE tends to cancel out its short-term variations and becomes more stable as temporal scale increases (Figure 2b) [*Song et al*., 2009, 2013]. Our analysis showed that most indicators were generally more effective in affecting LUE on the monthly scale than on the daily and 8 day scales (Figure 6). However, soil indicators explained LUE variations worse on the monthly scale than on the daily and 8 day scales, suggesting that the longer averaged SWC may not hold useful information to reflect the water stress on LUE. Soil water provides the direct water input for SPAC. However, our study showed poor relationships between LUE and SWC/SWS for most biomes, especially for forests and shrubs (Figures 4 and 7), suggesting that the flux-tower-based soil water measurement in the shallow soil layer (~30 cm) may not sufficiently capture the status of water supply for woody plants [*Reichstein et al*., 2002]. However, for grassland, SWC performed better than VPD in explaining LUE variations (Figure 7). Rooting depth and stem water storage may be the major controlling factors here. Direct measurement of rooting depth for natural ecosystems showed that forest and shrubs generally had deeper roots than grassland, although variations exist in different climate zones [*Canadell et al*., 1996; *Schenk and Jackson*, 2002]. For example, temperate grassland was shown to have a maximum rooting depth of 1.7 m, but roots of tropical deciduous forest could reach as deep as 3 m [*Schenk and Jackson*, 2002]. Compared to herbal plants, woody plants could have higher water accessibility via deep roots, and store more water in the stems [*Schenk and Jackson*, 2002; *Sims et al*., 2014] and thus decrease the sensitivity of LUE to the shallow soil moisture. Furthermore, the in situ soil moisture measurement from a single point location may not well represent the aggregate or horizontal moisture condition over the tower footprint, which is likely another cause of the poor correspondence between LUE and SWC. The threshold effect of soil moisture stress on LUE was expected to exist in different ecosystems [*Laio et al*., 2001]. However, our study found that SWS showed no obvious advantage in explaining LUE variations compared to SWC (Figure 4), suggesting the complexity of soil moisture stress on LUE. We recognized that the limited data records for SWC/SWS after screening as well as the use of global soil texture parameters to estimate SWS (i.e., equation (2)) may further contribute to uncertainties.

To explore the potential nonlinear effect of SWC on LUE, we further analyzed the relationships of LUE with different forms of SWC, i.e., polynomial SWC, $\log_{10}$(SWC), and SWC_{3PG} on three temporal scales. The R^2 between LUE and different forms are slightly higher on 8 day scale than on daily and monthly scales. However, considerable nonlinearity was not observed in those treatments (Figure 9). Currently, it is still a big challenge to fully simulate soil water dynamics by single or multibucket models [*Churkina et al*., 1999; *Song et al*., 2013]. Recently, NASA successfully launched an advanced Earth Science satellite called Soil Moisture Active Passive (SMAP) (http://smap.jpl.nasa.gov/), which provides not only the measured SWC in the top layer of the Earth's surface (~5 cm) but also value added SWC down to 1 m in depth taking account of additional ancillary input data, such as precipitation and root distribution [*Reichle et al*., 2014]. This mission provides unprecedented soil moisture information that could significantly enhance our understanding of global soil moisture stress on LUE.

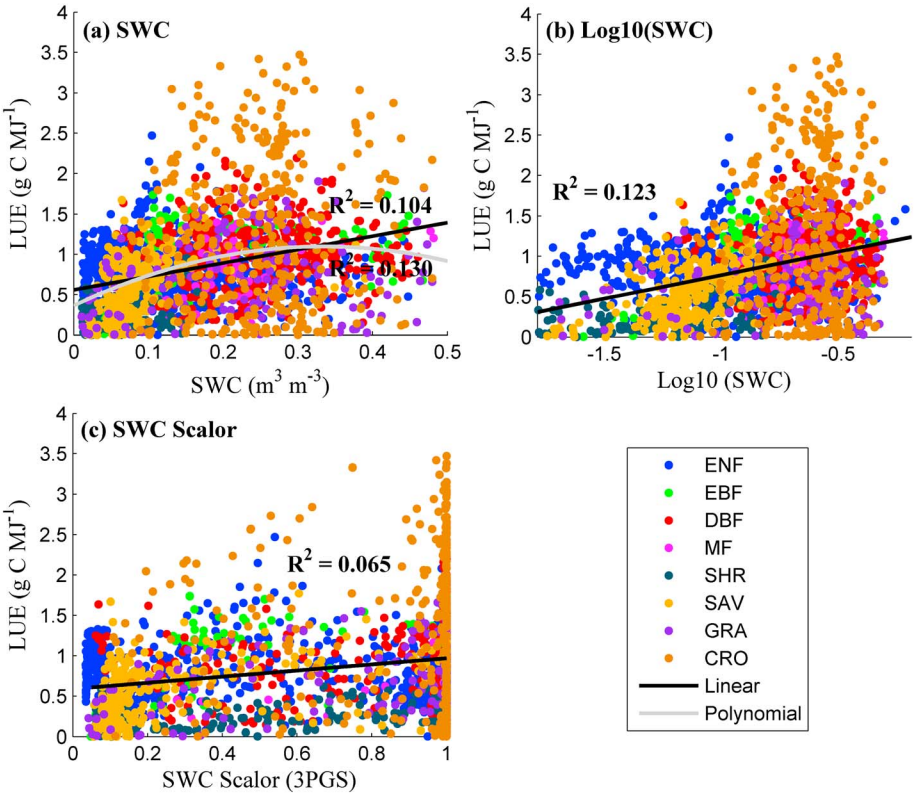

Figure 9. Scatterplots between LUE with (a) soil water content (SWC), (b) logarithm of SWC ($\log_{10}$(SWC)), and (c) SWC scalar from the 3PG Model [*Landsberg and Waring*, 1997] on the 8 day scale. Biome abbreviations are given in Table 1. The gray line in Figure 9a is the second-order polynomial fitting.

Moisture stress on plant is always coupled with temperature [*Brzostek et al*., 2014]. In this study, we screened the data by adopting the empirical thresholds of high and low temperatures for LUE [*Zhao and Running*, 2010], which was proved to be effective because no significant correlations between temperature and LUE data were found after the data filtering (results not shown). Nevertheless, no indicator was found to explain the variation of LUE stressed by moisture as much as one would have expected (Figures 2–7). In comparison, for example, on monthly scale, the representative indicators from atmosphere (VPD), soil (SWC), and plant (EF) moisture indicators only explained 20%, 6%, and 36% of LUE variations (Figure 6), respectively, reflecting the complexity of moisture stress on canopy photosynthesis [*Churkina et al*., 1999]. The limited ability of different indicators in tracking the effects of moisture stress on LUE may also be related to the following: (1) LUE uncertainties inherited from the tower-based estimation of GPP and MODIS FPAR; for example, tower-based GPP was subject to have 10%–30% errors due to the estimating and gap-filling methods used [*Reichstein et al*., 2005; *Schaefer et al*., 2012], while MODIS FPAR tended to be underestimated and displayed larger seasonal variations in old forests [*Serbin et al*., 2013]; (2) scaling errors between LUE over the tower footprint and site level in situ observations (e.g., SWC and precipitation) [*Schmid*, 2002]; (3) potential mismatches of temporal scale of data analysis and that of actual environmental stress, and (4) other uncontrolled factors, e.g., root distribution, drought adaption strategy, nutrient constraint, etc. [*Bréda et al*., 2006; *Reyer et al*., 2013; *Klein et al*., 2014]. Since our empirical analysis was conducted on the site basis, the goodness of fit may be little influenced if the above mentioned errors were systematic or evenly distributed within each site. However, if these errors were not systematic, e.g., randomly distributed within the site, the results would be affected. Further studies in more tightly controlled environment are needed to examine and validate our conclusions.

Currently, understanding and modeling drought effects on terrestrial ecosystem productivity is still a big challenge due to the complex ecophysiological responses of ecosystem to moisture stress [*Ruimy et al*., 1999; *Bréda et al*., 2006]. *Schaefer et al*. [2012] evaluated 26 GPP models with flux tower data over North

America and found that none of these models match estimated GPP within observed uncertainty. *Yuan et al.* [2014] compared seven LUE models with global flux tower data, and found that model performance differed substantially among ecosystem types. Both of these studies highlighted the uncertainties of the representation in moisture stress in the LUE models. Our study based on the global EC flux data covered the major moisture stress indicators used in the current LUE models, and the diverse responses of vegetation to moisture stress revealed by our study could help to improve the representation of moisture constraints and the associated accuracy in future global LUE-based productivity models.

5. Conclusions

Water and carbon fluxes are inherently coupled, and understanding how water stress affects plant growth is crucial to predict the responses of terrestrial ecosystems to global environmental changes. In this study, we investigated the effects of three groups of moisture indicators (i.e., atmosphere, soil, and plant) on LUE for a wide range of ecosystems on daily, 8 day, and monthly scales based on FLUXNET and MODIS data. After a series of data screening, we still found large variations in moisture stress on LUE among different ecosystems. In comparison, LUE is most responsive to plant moisture indicators (EF and LSWI), least responsive to soil moisture indicators (i.e., SWC and SWS) with the atmospheric moisture indicator (VPD) in between. LUE showed higher sensitivity to SWC than VPD only for grass. For evergreen forest, VPD showed better performance in explaining LUE variations than the plant moisture indicator, LSWI. Most moisture indicators were generally less effective in affecting LUE on the daily and 8 day scales than on the monthly scale. Our study highlights the complexity of moisture stress on LUE and suggests that a single moisture indicator or function in LUE models cannot capture the diverse responses of different vegetation to moisture stress. LUE models should consider the variability identified in this study to more realistically reflect the environmental controls on ecosystem functions.

Acknowledgments

The EC data set used in this study was from FLUXNET (http://www.fluxdata.org/), a global network of micrometeorological tower sites gathered from a series of regional networks including: CarboeuropeIP, AmeriFlux, Fluxnet-Canada, LBA, Asiaflux, Chinaflux, USCCC, Ozflux, Carboafrica, Koflux, NECC, TCOS-Siberia, and Afriflux. We appreciate the flux tower PIs who made these data freely available and all the other people who were involved in the tower field work. We would like to thank the Editor, the Associate Editor, and the anonymous reviewers who provide insightful and constructive comments on the manuscript. This research was financially supported by the U.S. National Science Foundation (DEB-1313756, USDA Forest Service-Joint Venture Agreement (14-JV-11330110-045) and Chinese Natural Science Foundation (31528004).

References

Agarwal, D. A., M. Humphrey, N. F. Beekwilder, K. R. Jackson, M. M. Goode, and C. van Ingen (2010), A data-centered collaboration portal to support global carbon-flux analysis, *Concurr. Comput*, *22*(17), 2323–2334.

Anav, A., P. Friedlingstein, C. Beer, P. Ciais, A. Harper, C. Jones, G. Murray-Tortarolo, D. Papale, N. C. Parazoo, and P. Peylin (2015), Spatio-temporal patterns of terrestrial gross primary production: A review, *Rev. Geophys.*, *53*, doi:10.1002/2015RG000483.

Asrar, G., M. Fuchs, E. Kanemasu, and J. Hatfield (1984), Estimating absorbed photosynthetic radiation and leaf area index from spectral reflectance in wheat, *Agron. J.*, *76*(2), 300–306.

Bacelar, E. L., J. M. Moutinho-Pereira, B. M. Gonçalves, C. V. Brito, J. Gomes-Laranjo, H. M. Ferreira, and C. M. Correia (2012), Water use strategies of plants under drought conditions, in *Plant Responses to Drought Stress*, pp. 145–170, Springer, Berlin.

Beer, C., M. Reichstein, E. Tomelleri, P. Ciais, M. Jung, N. Carvalhais, C. Rödenbeck, M. A. Arain, D. Baldocchi, and G. B. Bonan (2010), Terrestrial gross carbon dioxide uptake: Global distribution and covariation with climate, *Science*, *329*(5993), 834–838.

Bréda, N., R. Huc, A. Granier, and E. Dreyer (2006), Temperate forest trees and stands under severe drought: A review of ecophysiological responses, adaptation processes and long-term consequences, *Ann. For. Sci.*, *63*(6), 625–644.

Brzostek, E. R., D. Dragoni, H. P. Schmid, A. F. Rahman, D. Sims, C. A. Wayson, D. J. Johnson, and R. P. Phillips (2014), Chronic water stress reduces tree growth and the carbon sink of deciduous hardwood forests, *Global Change Biol.*, *20*, 2531–2539.

Campbell, G. S., and J. M. Norman (2012), *An Introduction to Environmental Biophysics*, Springer Science & Business Media, New York.

Canadell, J., R. Jackson, J. Ehleringer, H. Mooney, O. Sala, and E.-D. Schulze (1996), Maximum rooting depth of vegetation types at the global scale, *Oecologia*, *108*(4), 583–595.

Churkina, G., S. Running, A. Schloss, T. Intercomparison, and P. O. T. P. N. Model (1999), Comparing global models of terrestrial net primary productivity (NPP): The importance of water availability, *Global Change Biol.*, *5*(S1), 46–55.

Ciais, P., M. Reichstein, N. Viovy, A. Granier, J. Ogée, V. Allard, M. Aubinet, N. Buchmann, C. Bernhofer, and A. Carrara (2005), Europe-wide reduction in primary productivity caused by the heat and drought in 2003, *Nature*, *437*(7058), 529–533.

Crago, R. D. (1996), Conservation and variability of the evaporative fraction during the daytime, *J. Hydrol.*, *180*(1), 173–194.

Fang, Y., G. Sun, P. Caldwell, S. G. McNulty, A. Noormets, J. C. Domec, J. King, Z. Zhang, X. Zhang, and G. Lin (2015), Monthly land cover-specific evapotranspiration models derived from global eddy flux measurements and remote sensing data, *Ecohydrology*, doi:10.1002/eco.1629.

Fensholt, R., I. Sandholt, and M. S. Rasmussen (2004), Evaluation of MODIS LAI, fAPAR and the relation between fAPAR and NDVI in a semi-arid environment using in situ measurements, *Remote Sens. Environ.*, *91*(3), 490–507.

Friedl, M. A., D. Sulla-Menashe, B. Tan, A. Schneider, N. Ramankutty, A. Sibley, and X. Huang (2010), MODIS Collection 5 global land cover: Algorithm refinements and characterization of new datasets, *Remote Sens. Environ.*, *114*(1), 168–182.

Garbulsky, M. F., J. Peñuelas, D. Papale, J. Ardö, M. L. Goulden, G. Kiely, A. D. Richardson, E. Rotenberg, E. M. Veenendaal, and I. Filella (2010), Patterns and controls of the variability of radiation use efficiency and primary productivity across terrestrial ecosystems, *Global Ecol. Biogeogr.*, *19*(2), 253–267.

Jönsson, P., and L. Eklundh (2004), TIMESAT—A program for analyzing time-series of satellite sensor data, *Comput. Geosci.*, *30*(8), 833–845.

King, D. A., D. P. Turner, and W. D. Ritts (2011), Parameterization of a diagnostic carbon cycle model for continental scale application, *Remote Sens. Environ.*, *115*(7), 1653–1664.

Klein, T., D. Yakir, N. Buchmann, and J. M. Grünzweig (2014), Towards an advanced assessment of the hydrological vulnerability of forests to climate change-induced drought, *New Phytol.*, *201*(3), 712–716.

Knyazikhin, Y., J. Glassy, J. Privette, Y. Tian, A. Lotsch, Y. Zhang, Y. Wang, J. Morisette, P. Votava, and R. Myneni (1999), MODIS leaf area index (LAI) and fraction of photosynthetically active radiation absorbed by vegetation (FPAR) product (MOD15) algorithm theoretical basis document, edited.

Laio, F., A. Porporato, L. Ridolfi, and I. Rodriguez-Iturbe (2001), Plants in water-controlled ecosystems: Active role in hydrologic processes and response to water stress: II Probabilistic soil moisture dynamics, *Adv. Water Resour.*, *24*(7), 707–723.

Landsberg, J., and R. Waring (1997), A generalised model of forest productivity using simplified concepts of radiation-use efficiency, carbon balance and partitioning, *For. Ecol. Manage.*, *95*(3), 209–228.

McDowell, N., W. T. Pockman, C. D. Allen, D. D. Breshears, N. Cobb, T. Kolb, J. Plaut, J. Sperry, A. West, and D. G. Williams (2008), Mechanisms of plant survival and mortality during drought: Why do some plants survive while others succumb to drought?, *New Phytol.*, *178*(4), 719–739.

Medlyn, B. E. (1998), Physiological basis of the light use efficiency model, *Tree Physiol.*, *18*(3), 167–176.

Monteith, J. (1972), Solar radiation and productivity in tropical ecosystems, *J. Appl. Ecol.*, *9*(3), 747–766.

Mu, Q., M. Zhao, F. A. Heinsch, M. Liu, H. Tian, and S. W. Running (2007), Evaluating water stress controls on primary production in biogeochemical and remote sensing based models, *J. Geophys. Res.*, *112* G01012, doi:10.1029/2006JG000179.

Myneni, R., S. Hoffman, Y. Knyazikhin, J. Privette, J. Glassy, Y. Tian, Y. Wang, X. Song, Y. Zhang, and G. Smith (2002), Global products of vegetation leaf area and fraction absorbed PAR from year one of MODIS data, *Remote Sens. Environ.*, *83*(1), 214–231.

Nemani, R. R., C. D. Keeling, H. Hashimoto, W. M. Jolly, S. C. Piper, C. J. Tucker, R. B. Myneni, and S. W. Running (2003), Climate-driven increases in global terrestrial net primary production from 1982 to 1999, *Science*, *300*(5625), 1560–1563.

Ocheltree, T., J. Nippert, and P. Prasad (2014), Stomatal responses to changes in vapor pressure deficit reflect tissue-specific differences in hydraulic conductance, *Plant Cell Environ.*, *37*(1), 132–139.

Piao, S., S. Sitch, P. Ciais, P. Friedlingstein, P. Peylin, X. Wang, A. Ahlström, A. Anav, J. G. Canadell, and N. Cong (2013), Evaluation of terrestrial carbon cycle models for their response to climate variability and to CO_2 trends, *Global Change Biol.*, *19*(7), 2117–2132.

Potter, C. S., J. T. Randerson, C. B. Field, P. A. Matson, P. M. Vitousek, H. A. Mooney, and S. A. Klooster (1993), Terrestrial ecosystem production: A process model based on global satellite and surface data, *Global Biogeochem. Cycles*, *7*(4), 811–841, doi:10.1029/93GB02725.

Reichle, R., R. Koster, G. De Lannoy, W. Crow, and J. Kimball (2014), Soil moisture active passive (SMAP): Level 4 surface and root zone soil moisture (L4_SM) data product algorithm theoretical basis document. [Available at http://smap-archive.jpl.nasa.gov/files/smap2/L4_SM_RevA.pdf, Access Date: 04-15-2015.]

Reichstein, M., J. D. Tenhunen, O. Roupsard, J. M. Ourcival, S. Rambal, F. Miglietta, A. Peressotti, M. Pecchiari, G. Tirone, and R. Valentini (2002), Severe drought effects on ecosystem CO_2 and H_2O fluxes at three Mediterranean evergreen sites: Revision of current hypotheses?, *Global Change Biol.*, *8*(10), 999–1017.

Reichstein, M., E. Falge, D. Baldocchi, D. Papale, M. Aubinet, P. Berbigier, C. Bernhofer, N. Buchmann, T. Gilmanov, and A. Granier (2005), On the separation of net ecosystem exchange into assimilation and ecosystem respiration: Review and improved algorithm, *Global Change Biol.*, *11*(9), 1424–1439.

Reyer, C. P., S. Leuzinger, A. Rammig, A. Wolf, R. P. Bartholomeus, A. Bonfante, F. de Lorenzi, M. Dury, P. Gloning, and R. Abou Jaoudé (2013), A plant's perspective of extremes: Terrestrial plant responses to changing climatic variability, *Global Change Biol.*, *19*(1), 75–89.

Ruimy, A., L. Kergoat, A. Bondeau, T. Intercomparison, and P. O. T. P. N. Model (1999), Comparing global models of terrestrial net primary productivity (NPP): Analysis of differences in light absorption and light-use efficiency, *Global Change Biol.*, *5*(S1), 56–64.

Running, S. W. (2012), A measurable planetary boundary for the biosphere, *Science*, *337*(6101), 1458–1459.

Schaefer, K., C. R. Schwalm, C. Williams, M. A. Arain, A. Barr, J. M. Chen, K. J. Davis, D. Dimitrov, T. W. Hilton, and D. Y. Hollinger (2012), A model-data comparison of gross primary productivity: Results from the North American Carbon Program site synthesis, *J. Geophys. Res.*, *117*, G03010, doi:10.1029/2012JG001960.

Schenk, H. J., and R. B. Jackson (2002), The global biogeography of roots, *Ecol. Monogr.*, *72*(3), 311–328.

Schmid, H. P. (2002), Footprint modeling for vegetation atmosphere exchange studies: A review and perspective, *Agric. For. Meteorol.*, *113*(1), 159–183.

Serbin, S. P., D. E. Ahl, and S. T. Gower (2013), Spatial and temporal validation of the MODIS LAI and FPAR products across a boreal forest wildfire chronosequence, *Remote Sens. Environ.*, *133*, 71–84.

Shabanov, N., Y. Wang, W. Buermann, J. Dong, S. Hoffman, G. Smith, Y. Tian, Y. Knyazikhin, and R. Myneni (2003), Effect of foliage spatial heterogeneity in the MODIS LAI and FPAR algorithm over broadleaf forests, *Remote Sens. Environ.*, *85*(4), 410–423.

Sims, D. A., E. R. Brzostek, A. F. Rahman, D. Dragoni, and R. P. Phillips (2014), An improved approach for remotely sensing water stress impacts on forest C uptake, *Global Change Biol.*, *9*(20), 2856–2866.

Siqueira, M., G. Katul, and A. Porporato (2009), Soil moisture feedbacks on convection triggers: The role of soil-plant hydrodynamics, *J. Hydrometeorol.*, *10*(1), 96–112.

Song, C., G. Katul, R. Oren, L. E. Band, C. L. Tague, P. C. Stoy, and H. R. McCarthy (2009), Energy, water, and carbon fluxes in a loblolly pine stand: Results from uniform and gappy canopy models with comparisons to eddy flux data, *J. Geophys. Res.*, *114*, G04021, doi:10.1029/2009JG000951.

Song, C., M. P. Dannenberg, and T. Hwang (2013), Optical remote sensing of terrestrial ecosystem primary productivity, *Prog. Phys. Geogr.*, *37*(6), 834–854.

Sun, G., P. Caldwell, A. Noormets, S. G. McNulty, E. Cohen, J. Moore Myers, J. C. Domec, E. Treasure, Q. Mu, and J. Xiao (2011), Upscaling key ecosystem functions across the conterminous United States by a water-centric ecosystem model, *J. Geophys. Res.*, *116*, G00J05, doi:10.1029/2010JG001573.

Tuzet, A., A. Perrier, and R. Leuning (2003), Stomatal control of photosynthesis and transpiration: Results from a soil-plant-atmosphere continuum model, *Plant Cell Environ.*, *26*, 1097–1116.

Vicente-Serrano, S. M., C. Gouveia, J. J. Camarero, S. Beguería, R. Trigo, J. I. López-Moreno, C. Azorín-Molina, E. Pasho, J. Lorenzo-Lacruz, and J. Revuelto (2013), Response of vegetation to drought time-scales across global land biomes, *Proc. Natl. Acad. Sci. U.S.A.*, *110*(1), 52–57.

Wei, S., Y. Dai, Q. Duan, B. Liu, and H. Yuan (2014), A global soil data set for Earth system modeling, *J. Adv. Model. Earth Syst.*, *6*, 249–263, doi:10.1002/2013MS000293.

Williams, M., B. E. Law, P. M. Anthoni, and M. H. Unsworth (2001), Use of a simulation model and ecosystem flux data to examine carbon–water interactions in ponderosa pine, *Tree Physiol.*, *21*(5), 287–298.

Wu, C., and J. Chen (2012), The use of precipitation intensity in estimating gross primary production in four northern grasslands, *J. Arid Environ.*, *82*, 11–18.

Xiao, X., D. Hollinger, J. Aber, M. Goltz, E. A. Davidson, Q. Zhang, and B. Moore III (2004), Satellite-based modeling of gross primary production in an evergreen needleleaf forest, *Remote Sens. Environ.*, *89*(4), 519–534.

Xie, J., G. Sun, H. S. Chu, J. Liu, S. G. McNulty, A. Noormets, R. John, Z. Ouyang, T. Zha, and H. Li (2014), Long-term variability in the water budget and its controls in an oak-dominated temperate forest, *Hydrol. Processes*, *28*(25), 6054–6066.

Yuan, W., S. Liu, G. Zhou, G. Zhou, L. L. Tieszen, D. Baldocchi, C. Bernhofer, H. Gholz, A. H. Goldstein, and M. L. Goulden (2007), Deriving a light use efficiency model from eddy covariance flux data for predicting daily gross primary production across biomes, *Agric. For. Meteorol.*, *143*(3), 189–207.

Yuan, W., W. Cai, J. Xia, J. Chen, S. Liu, W. Dong, L. Merbold, B. Law, A. Arain, and J. Beringer (2014), Global comparison of light use efficiency models for simulating terrestrial vegetation gross primary production based on the LaThuile database, *Agric. For. Meteorol.*, *192*, 108–120.

Zhang, Y., C. Song, K. Zhang, X. Cheng, L. E. Band, and Q. Zhang (2014), Effects of land-use/land-cover and climate changes on terrestrial net primary productivity in the Yangtze River Basin, China from 2001 to 2010, *J. Geophys. Res. Biogeosci.*, *6*, 1092–1109, doi:10.1002/2014JG002616.

Zhao, M., and S. W. Running (2010), Drought-induced reduction in global terrestrial net primary production from 2000 through 2009, *Science*, *329*(5994), 940–943.

Zhao, M., F. A. Heinsch, R. R. Nemani, and S. W. Running (2005), Improvements of the MODIS terrestrial gross and net primary production global data set, *Remote Sens. Environ.*, *95*(2), 164–176.